Hybrid DFT-spread OFDM-Digital Filter Multiple Access PONs for Converged 5G Networks

Dong, Y. X.; Jin, W.; Giddings, R. P.; O'Sullivan, M.; Tipper, A.; Durrant, T.; Tang, J. M.

IEEE Journal of Optical Communications and Networking

Hybrid DFT-spread OFDM-Digital Filter Multiple Access PONs for Converged 5G Networks

Y.X. Dong, W. Jin, R.P. Giddings, M. O'Sullivan, A. Tipper, T. Durrant, and J.M. Tang

Abstract— **Hybrid discrete Fourier transform (DFT)-spread orthogonal frequency division multiplexing (OFDM)-digital filter multiple access (DFMA) passive optical networks (PONs) are proposed, for the first time, where digital signal processing (DSP)-based digital filtering is applied to individual DFT-spread OFDM signals from various optical network units (ONUs), and a single FFT operation and its following data recovery processes are implemented in a pipelined approach in the optical line terminal (OLT). The proposed networks maintain all salient features associated with previously reported hybrid OFDM-DFMA PONs, more importantly, they additionally reduce the upstream signal peak-to-average power ratios (PAPRs) by >2dB. As a direct result, in comparison with the hybrid OFDM-DFMA PONs, the proposed PONs increase the upstream system power budget by >3dB and reduce the minimum required DAC/ADC quantization bits by at least 1 bit.**

Index Terms— **Passive optical networks (PONs), digital signal processing (DSP), digital filter multiple access, OFDM, DFT-spread OFDM.**

I. INTRODUCTION

TO achieve the targeted 5G performances specifications including significantly increased signal transmission capacities, massive machine-type communications as well as ultra-reliable low-latency real-time services [1, 2], a wide diversity of unprecedented technical challenges across all layers must be addressed, among which non-incremental solutions should be developed to seamlessly converge, in a cost-effective manner, separately implemented and operated legacy optical and wireless networks [3]. To deliver such an objective, passive optical networks (PONs) are widely considered as one of the most promising solutions [4]. To enable the PON-based converged 5G networks to offer on-demand heterogeneous services in a multiple virtual operator-shared environment, software defined networking (SDN) is vital to transfer the present inflexible and vendor-locked network infrastructure into an agile and flexible platform [5, 6]. Furthermore, it is also greatly advantageous if the abovementioned flexible networks have good backward compatibility to existing orthogonal frequency division multiplexing (OFDM)-based 4G networks [7].

To address the abovementioned challenges, recently novel hybrid OFDM-digital filter multiple access (DFMA) PONs [8] capable of providing excellent transparency to OFDM-based 4G networks has been proposed, where digital signal processing (DSP)-based software-reconfigurable digital filtering is applied to individual OFDM signals produced by each optical network unit (ONU), while in the corresponding optical line terminal (OLT), a single FFT operation and its following data recovery processes are implemented in a pipelined approach, regardless of the ONU count accommodated by the network. Compared to the conventional OFDM PONs, such a network not only extends the highly desirable SDN network control functions to the physical layer, but also considerably enhances the upstream performance robustness to practical transceiver/system impairments. In addition, compared to the DFMA PONs, the hybrid OFDM-DFMA PONs also greatly relax the stringent requirements on the high DSP complexity of shaping filters (SFs) in the ONUs, and more importantly, they completely eliminate the match filtering operations in the OLT, thus resulting in greatly reduced OLT DSP complexity and considerably enhanced flexibility [8].

It is well known that OFDM's inherent multi-subcarrier modulation feature can cause the time-domain waveforms associated with various subcarriers to be added up coherently after the IFFT operation. This gives an OFDM signal a high peak-to-average power ratio (PAPR) [9]. A high PAPR not only requires large dynamic operation ranges of electrical/optical devices but also produces high quantization noise for fixed quantization bits. The quantization noise effect is particularly strong when current market-available high-speed digital-to-analog converters/ analog-to-digital converters (DACs/ADCs) are implemented, as their performances are bit resolution-limited. In addition, when transmitting over fibre systems, a high PAPR signals may also impose enhanced system performance sensitivity to fibre nonlinearities. Therefore, from the cost-effective transceiver design point of view, it is greatly beneficial if the generated OFDM signals have relatively low PAPRs.

To reduce the PAPR of an OFDM signal, apart from the widely adopted simple clipping technique, several other techniques have also been reported including selective mapping (SLM) and partial transmit sequences (PTS) [10, 11], both of
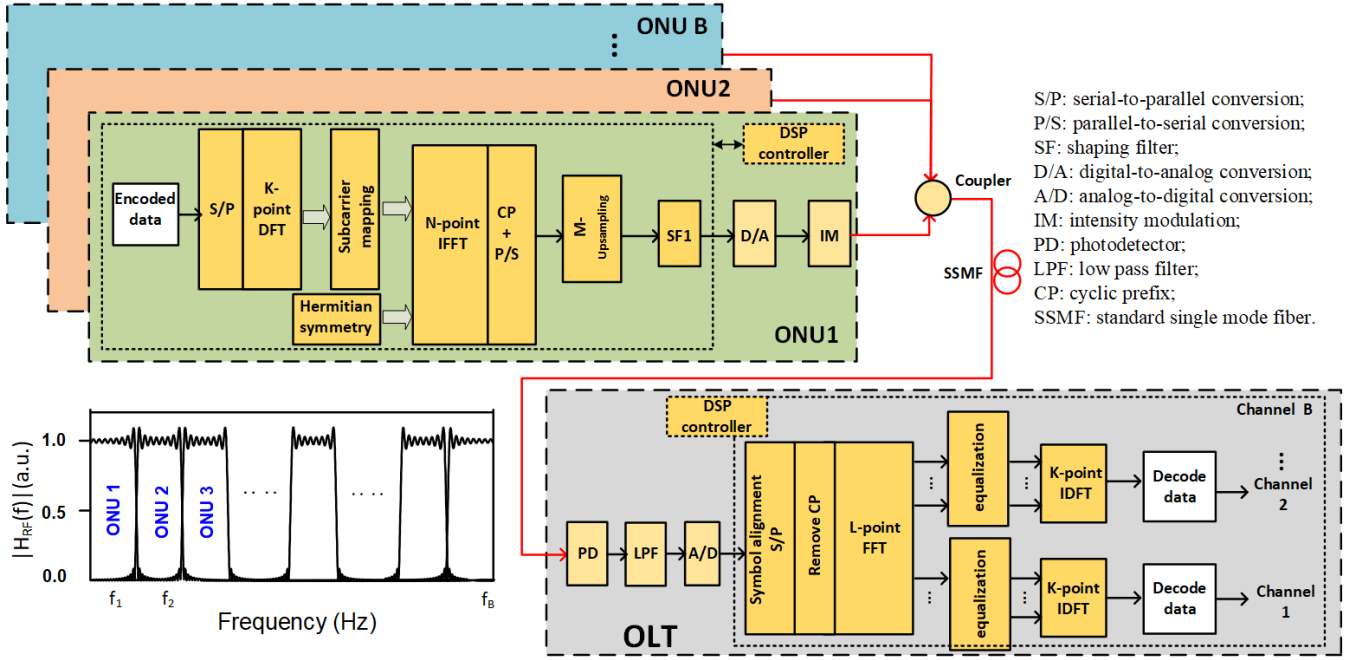
Fig. 1 Proposed hybrid DFT-spread OFDM-DFMA IMDD PONs simultaneously accommodating B ONUs.

which, however, suffer from high computational complexity. Apart from that, the SLM-induced PAPR reduction strongly depends upon the total number of employed IDFT blocks, whilst the PTS requires a large bandwidth overhead. Given the fact that the discrete Fourier transform (DFT) can spread the spectrum of the subcarriers and subsequently decrease the probability of independently modulated subcarrier's waveforms being added up coherently by the IFFT operation, the PAPRs of the produced signals can thus be reduced considerably [12, 13]. In the long-term evolution (LTE) mobile standards, DFT-spread OFDM is adopted due to its effectiveness in reducing the PAPRs and relatively low DSP complexity [12-14].

To effectively address the PAPR challenge associated with the hybrid OFDM-DFMA PON and further enhance its compatibility to existing 4G network, it is great beneficial if the DFT-spread technique is utilized in the hybrid OFDM-DFMA PON. In this paper, hybrid DFT-spread OFDM-DFMA PONs are proposed and numerically explored for the first time. The proposed PONs are shown to maintain all the features of the hybrid OFDM-DFMA PONs and further improve system transmission performance flexibility. We show that for upstream 13.125Gb/s signals transmitted over 25km SSMF PON systems based on intensity modulation and direct detection (IMDD), the proposed technique saves 1 quantization resolution bit and increases the system power budget by 3dB, compared to the previously published hybrid OFDM-DFMA PONs [8].

This paper is organized as following: in Section II, a detailed theoretical model of the proposed hybrid DFT-spread OFDM-DFMA PONs is developed, which considerably extends the previously reported hybrid OFDM-DFMA PON model [8]. From the physical PON operation point of view, the hybrid DFT-spread OFDM-DFMA PON model confirms the feasibility of utilizing DFT-spread OFDM in hybrid OFDM-DFMA PONs. Section III presents numerically simulated upstream transmission performances of the proposed PONs and their corresponding optimum transceiver designs. It is shown that, apart from the aforementioned >3dB increase in upstream system power budget and >1-bit reduction in minimum required DAC/ADC quantization bits, the proposed PON also gives rise to a >2dB reduction in upstream signal peak-to-average power ratio (PAPR). Moreover, in this section, detailed explorations of the impact of DAC/ADC quantization bit and clipping ratio on the upstream transmission performance are also undertaken for optimum transceiver designs. The results presented in this paper indicate that the proposed PONs not only enhances the upstream transmission performance but also reduces the hardware/DSP complexity, thus this work has potential of paving a valuable path for practical applications in converged 5G networks. Finally, the paper is summarized in Section IV.

II. PRINCIPLE OF HYBRID DFT-SPREAD OFDM-DFMA PONs

Fig.1 depicts the diagram of the proposed hybrid DFT-spread OFDM-DFMA IMDD PONs. Here special attention is focused on the more challenging multipoint-to-point upstream transmission only. As illustrated in Fig.1, the upstream optical signals from B ONUs, labelled as 1st, 2nd … B th ONU, are passively combined for upstream transmission. At each ONU arbitrarily encoded samples are converted from serial to parallel, and a K-point DFT operation is then applied to produce K spectrum spread samples. The obtained K-point DFT-spread signal $a(k')$ is expressed as:

$$a(k') = \sum_{k''=-\frac{K}{2}}^{\frac{K}{2}-1} d(k'')e^{-j\frac{2\pi k'k''}{K}},$$

$$k' = 0,1, \ldots, K - 1 \qquad (1)$$

where $d(k'')$ is the time-domain sample sequence.

In the subsequent IFFT operation, the first subcarrier is set at zero, and the K spectrum spread samples are mapped onto the K respective subcarriers, while all the remaining unused subcarriers are set to be zeros to produce $\frac{N}{2}$ subcarriers in total, here $K \leq \frac{N}{2} - 1$, the parallel sample sequence $c(k)$ can be expressed as:

$$c(k) = \begin{cases} a(k'), for\ K\ subcarriers \\ 0,\ for\ other\ subcarriers \end{cases}, k = 0,1, \ldots, \frac{N}{2} - 1 \quad (2)$$

After that, the Hermitian symmetry is applied to generate a real-valued DFT-spread OFDM signal after the N-point IFFT operation. The mth OFDM symbol generated by the N-point IFFT of the set of N subcarriers can be written as:

$$x_m(n) = \sum_{k=-\frac{N}{2}}^{\frac{N}{2}-1} c_m(k) e^{j\frac{2\pi k(n-mN)}{L}},$$
$$n = 0, \ldots, L - 1; m = 0,1, \ldots \qquad (3)$$

where $c_m(k)$ is the mth data block of $c(k)$ after enforcing Hermitian symmetry, L is the symbol length in samples. For conventional OFDM without any up-sampling, we have $L=N$. As these subcarriers are localized mapping [12], for a given N, a large K gives rise to an enhanced PAPR reduction. Following the IFFT operation, the DFT-spread OFDM signal is up-sampled by a factor of M, thus an up-sampled OFDM symbol contains $L = MN$ samples, which then passes through a digital orthogonal shaping filter (SF) to locate the signal at a desired spectral region. Using an ideal shaping filter that has a rectangle-shaped frequency response, the filtered signal in the bth channel can be expressed as [8]:

$$x_{m,b}(n) = \frac{1}{M} \sum_{n=-N}^{N-1} c'_{m,b}(k) e^{j2\pi n \left(\frac{k+bN\frac{k}{|k|}}{L} \right)}$$
$$c'_{m,b}(k) = \{c_{m,b}(k)_{neg}, c_{m,b}(k)_{pos}\} \qquad (4)$$

where $c_{m,b}(k)$ represents the mth data block of $c(k)$ in the bth channel, $c_{m,b}(k)_{pos}$ ($c_{m,b}(k)_{neg}$) refers to the subcarriers located at positive (negative) bin, which satisfies [8]:

$$c_{m,b}(k)_{neg} = c_{m,b}(k)_{pos} = c_{m,b}(k) \qquad (5)$$

Finally, the digitally filtered signal samples $x_{m,b}(n)$ are fed to a DAC to generate an analogue electrical signal $x_b(t)$. After that, optical intensity modulation can be performed, as seen in Fig.1. The coupled optical field from a total number of B ONUs can be expressed as:

$$S_{opt}(t) = \sum_{b=0}^{B-1} \left[\sigma_b(t) e^{j\beta_b(t)} \cdot \sqrt{1 + \zeta_b * x_b(t)} \right] e^{i2\pi f_{opt} t}$$
$$(6)$$

where f_{opt} is the optical carrier frequency and ζ_b is the optical intensity modulation index of the bth channel, $\sigma_b(t)$ and $\beta_b(t)$ take into account the optical intensity modulation impacts on the amplitude and phase of the bth optical signal.

To simplify the theoretical analyses for the proposed hybrid DFT-spread OFDM-DFMA PONs, similar to the treatments reported in [8], linear transmission systems are assumed in this section only and numerical simulations are performed in Section III to examine the feasibility of the proposed technique in practical non-linear PON transmission systems. Under these assumptions, in the OLT, after optical-electrical conversion and an ADC, the received signals emitted from a total number of B ONUs can be expressed as:

$$y(n) = \sum_{b=0}^{B-1} x_{m,b}(n) = \frac{1}{M} \left(\sum_{b=0}^{B-1} \sum_{k=-N}^{N-1} c'_{m,b}(k) e^{j\frac{2\pi\left(k+bN\frac{k}{|k|}\right)n}{L}} \right)$$
$$(7)$$

Let $\rho = k + bN\frac{k}{|k|}$, the following expressions can then be satisfied:

$$\begin{cases} k \in [-N, N-1] \\ b \in [0, B-1] \\ \rho \in [-BN, BN-1] \end{cases} \qquad (8)$$

Thus the received signal $y(n)$ can be rewritten as:

$$y(n) = \frac{1}{M} \sum_{\rho=-BN}^{BN-1} c'_m(\rho) e^{j\frac{2\pi\rho n}{L}}$$
$$c'_m(\rho) = c'_{m,b}(k) \qquad (9)$$

Eq.(9) indicates that the received signal can be processed by the L-point IFFT operation with $L= 2BN$. As such, in the OLT, the L-point FFT can be applied to $y(n)$ to recover the data sequence $c'_{m,b}(k)$ without implementing the digital filtering process required by conventional DFMA systems. The elimination of the OLT-embedded digital filtering process significantly reduces the OLT DSP complexity [8]. After the FFT operation, the obtained data sequence can be expressed as:

$$c'_m(\rho) = \sum_{n=-BN}^{BN-1} y(n) e^{-j\frac{2\pi\rho n}{L}}$$
$$(10)$$

In the OLT, as shown in Fig.1, after the photodetector, LPF and ADC, the obtained digital samples are firstly converted into parallel samples corresponding in length to one symbol period

by a deserialiser. Similar to conventional OFDMA PONs [15], a symbol alignment block is employed to achieve symbol alignment and compensate for any possible symbol offset. The cyclic prefix (CP) can then be removed, thus the remaining L time-domain samples are obtained for each symbol. After the following L-point FFT operation, the FFT-output sample sequence $\{c'_m(\rho)\} = \{c'_m(0), c'_m(1), \ldots, c'_m(L-1)\}$ is obtained [8]. To identify the corresponding spectrum spread subcarriers $\{a_b\}$ from $\{c'_m(\rho)\}$ for a targeted ONU b, Eq.(11) is utilized, which presents the rules of the spread-subcarrier selection, and the corresponding spread-subcarrier index z is given in Eq.(12):

$$\{a_b\} = \left[\overbrace{c'_m(z), c'_m(z+1) \ldots, c'_m\left(z+\frac{N}{2}-1\right)}^{the\ first\ and\ \frac{N}{2}-1\ data-bearing\ subcarriers}, \underbrace{c'_m(z+N-1), c'_m(z+N-2), \ldots, c'_m\left(z+\frac{N}{2}\right)}_{\frac{N}{2}\ conjugate\ subcarriers} \right]$$

$$b = 0,1,\ldots,B-1 \quad (11)$$

$$z = \begin{cases} 0, & b = 0 \\ \frac{L}{2} + (B-b-1)\cdot N, & b \geq 1 \end{cases} \quad (12)$$

After having identified the spectrum spread subcarriers from the bth ONU, standard OFDM equalization [15] can be utilized for signal recovery, followed by the K-point IDFT in Eq.(13):

$$d(k'') = \sum_{k'=-\frac{K}{2}}^{\frac{K}{2}-1} a(k')e^{j\frac{2\pi k'k''}{K}}$$

$$(13)$$

where $a(k')$ is the parallel samples selected from $\{a_b\}$ through the corresponding K subcarrier positions, and the IDFT-operation generated data $d(k'')$ is ready for the further decoding operations to recovery the transmitted information.

From the above-described digital signal processing procedures in both the ONU and the OLT, it is easy to understand the following aspects: 1) the hybrid DFT-spread OFDM-DFMA PONs retain the advantages of previously-reported hybrid OFDM-DFMA PONs, such as reduced OLT DSP complexity; 2) as will be demonstrated in Section III, for practical implementation in 5G networks, the proposed hybrid DFT-spread OFDM-DFMA PONs further improve transmission system performance and reduce overall network installation expenditures, and 3) the downlink operation of the proposed hybrid DFT-spread OFDM-DFMA PONs is identical to those associated with DFMA PONs and OFDMA PONs when the corresponding digital filtering processes in both the OLT and ONUs are switched on and off respectively. This statement also holds true for the hybrid OFDM-DFMA PON downlink operation. Clearly, such a PON operation feature further enhances the network flexibility and adaptability to practical hardware impairments and/or dynamic network traffic status. As detailed downlink operation characteristics of DFMA
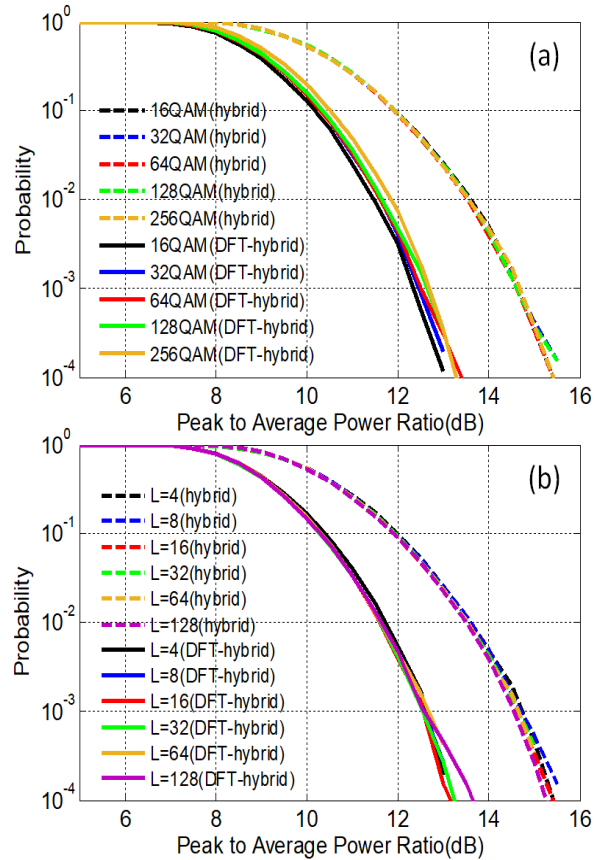

Fig.2 CCDF curves of channel 1: (a) for different QAM modulation formats and fixed filter lengths of 64; (b) for different filter lengths from 4 to 128 and adopted signal modulation formats of 64QAM .

PONs and OFDMA PONs have already been reported in [9] and [15] respectively, only the more challenging upstream operation of the proposed PONs is thus explored in the paper.

III. HYBRID DFT-SPREAD OFDM-DFMA PONs PERFORMANCE

In this section, numerical simulations of the upstream performances of 25 km SSMF IMDD hybrid DFT-spread

TABLE I
LIST OF PARAMETERS

PARAMETER	VALUE	PARAMETER	VALUE
DAC/ADC sample rate	12.5 GS/s	DAC/ADC resolution	6 bits
Clipping ratio	14dB	Cyclic Prefix per channel	25%
Modulation formats	64QAM	Total number of IFFT points of each channel	32
Transmitted optical power	0dBm	Received optical power	-6dBm
SSMF length	25km	Up sampling factor M	4
PIN detector bandwidth	12.5GHz	PIN detector sensitivity	-19dBm
Fiber dispersion	17 ps/nm/km	Fiber dispersion slope	0.07 ps/nm/km
Fiber Kerr coefficient	2.35e-20 m²/W	Fiber loss	0.2 dB/km
SF filter length/ alpha factor	64/0	Hybrid OFDM-DFMA FFT size	128

OFDM-DFMA PONs (abbreviated as 'DFT-hybrid' case) are undertaken, and performance comparisons are made with the previously reported hybrid OFDM-DFMA PONs (abbreviated as 'hybrid' case) to highlight the unique advantages associated with the proposed technique. The approach reported in [8] is adopted for OFDM signal generation/detection and the digital filter construction in the ONUs. Optical fibre transmission is simulated using VPI Transmission maker. Given the fact that, according to our numerical results, the ONU-count dependent upstream performance of the proposed hybrid DFT-spread OFDM-DFMA PONs is very similar to the previously published hybrid OFDM-DFMA PONs [8], for simplicity but without losing generality, two ONUs are considered throughout this paper. Each ONU employs an ideal optical intensity modulator for E-O conversion as reported in [8], thus the parameters of σ_b and β_b included in Eq. (6) are taken to be 1 and 0 respectively, and the intensity modulation index is set to 0.99. In addition, as ideal intensity modulation does not introduce the optical beat interference effect, no optical frequency offset and polarization mismatch between ONU carriers are considered, as these effects are not significant over typical operation conditions for the application scenarios of interest of this paper [16]. In implementing the digital filtering process in the considered ONUs, only in-phase filters [8] are utilised at different RF central frequencies governed by Eq.(14):

$$f_k = (2b+1)\frac{f_s}{2M}, b = 0,1,\dots,B-1 \quad (14)$$

where f_s is the DAC/ADC sampling speed. The locations of the in-phase filters assigned to individual ONUs are illustrated at the bottom left of Fig.1. To enable the considered two ONUs to occupy the entire spectral region, an up-sampling factor M is taken to be 4, thus the involved digital filter central frequencies satisfy: $f_1 = f_s/8$ and $f_2 = 3 \times f_s/8$. Generally speaking, the minimum M factor for supporting a total B ONUs should be $2B$ [9]. In generating the required real-valued OFDM signals, a 32-point IFFT (N=32) is used, thus the maximum usable data-bearing subcarriers in each ONU is 15. To reduce the channel interferences between the two ONUs and maximise their signal transmission capacity, ONU1(ONU2) has fourteen 64-QAM encoded data-bearing subcarriers, i.e., from subcarrier 2 to 15(3 to 16), thus the DFT block size is K=14. For both the hybrid and DFT-hybrid cases, their PAPR developing trends are almost independent of signal modulation format, as seen in Fig.2(a). In this figure, their cumulative distribution function (CCDF) curves for various modulation formats varying from 16QAM to 256QAM are presented for Channel 1, Channel 2's PAPR curves are not plotted in the figure as they are similar to Channel 1. As such, for all numerical simulations, the signal modulation format of 64QAM is adopted in exploring the upstream performances of the proposed PONs. All other parameters are listed in Table I, and the total aggregated signal transmission capacity is 13.125Gb/s for both the hybrid case and the DFT-hybrid case. The signal bit rate R_b of each individual ONU can be calculated using the formula below:

$$R_b = \frac{f_s \sum_{k=1}^{S} n_{kb}}{N(1+C_p)M} \quad (15)$$

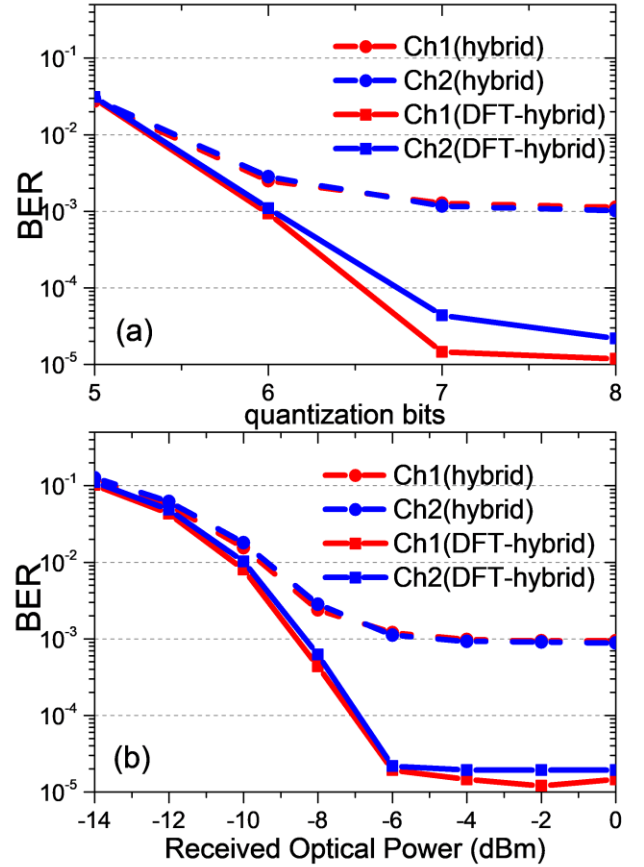where n_{kb} represents the number of binary information bits

Fig. 3 (a) BER versus quantization bits; (b) BER versus received optical power when resolution bits are 7.

conveyed by the k-th subcarrier within one OFDM symbol period, S stands for the total number of data-bearing subcarriers and C_p is the overhead parameter associated with the cyclic prefix and training sequence. After up-sampling, the signal bandwidth of each ONU is $f_s/(2 \cdot M)$. At the OLT side, to avoid the aliasing effect, an ideal electrical filter with a bandwidth of 6.25GHz is utilized to remove unwanted high frequency out-of-band noise before the ADC.

The PAPR performances of the hybrid OFDM-DFMA PONs with and without DFT-spread are respectively explored utilizing the parameters described above, and their CCDF curves are plotted in Fig.2. It shows that at the adopted 14dB clipping ratio region, DFT-spread gives rise to a PAPR reduction as large as ≥ 2dB. In addition, as expected, such DFT-spread induced PAPR reductions are independent of both signal modulation format and digital filter length, as shown in Fig.2(a) and Fig.2(b) respectively. As a direct result of the digital filter length-independent PAPR reductions, the DFT-hybrid case also demonstrates almost identical upstream transmission performances over a large digital filter length variation range, similar to those reported in [8]. Since the performances of the typical hybrid OFDM-DFMA PONs are mainly limited by digital filter-induced signal distortions [8], to highlight the effectiveness of the DFT-spread technique by effectively minimizing the digital filter impairments, in this paper a fixed digital filter length of 64 is adopted, as listed in Table I.

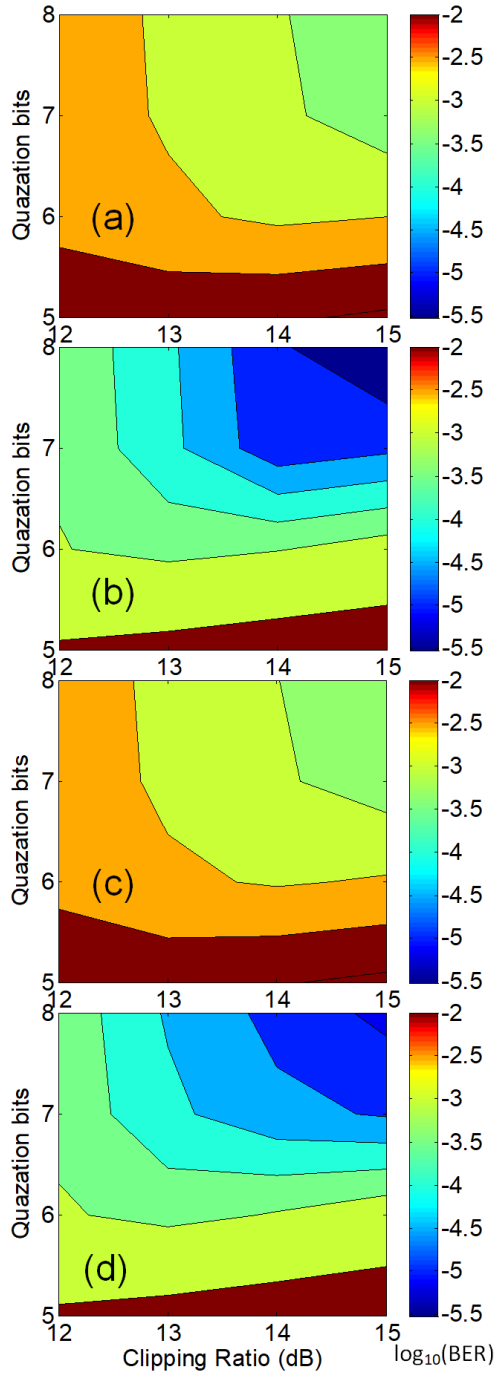The abovementioned considerable PAPR reduction not only

Fig. 4 BER contour versus quantization bit resolution and clipping ratio,(a) channel 1 in hybrid case; (b) channel 1 in DFT-hybrid case; (c) channel 2 in hybrid case; (d) channel 2 in DFT-hybrid case.

increased to 7. Therefore, the performance tolerance to the quantization noise is improved by the DFT-spread technique. Such improvement is highly preferable for cost-sensitive application scenarios where low-cost DAC/ADCs with relatively low resolution bits and power consumptions can be applied. In addition, for a specific DAC/ADC resolution of 7 bits, the improved transmission performance by the DFT-spread technique is presented in Fig.3 (b). It can be seen that the DFT-hybrid case can improve the system power budget by 3dB compared to the hybrid case. Such improvement is mainly due to the fact that the quantization noise is considerably decreased for the DFT-spread OFDM signals. In addition, this power budget improvement further enhances the network capability of accommodating higher traffic load and/or increasing the network coverage.

To extensively explore the dynamics between bit resolution and clipping ratio for the optimum design of transceivers incorporated in the hybrid DFT-spread OFDM-DFMA PONs, Fig.4 is presented where the obtained BER contours are plotted against clipping ratio and quantization bit. It can be seen that for quantization bits ranging from 6 to 8, to maintain the BERs below < 1E-3, clipping ratios should always be >14dB for the hybrid case, while for the DFT-hybrid case, such a clipping ratio value is decreased to 12dB over the same quantization bit variation region. The results in Fig. 3 and Fig. 4 also imply that: 1) the similar transmission performance of the considered ONUs with/without incorporating the DFT-spread technique indicates that the performance improvements induced by the DFT-spread technique is independent of channel frequency locations, which are valuable for practical multi-channel applications; 2) the DFT-spread technique allows the transceivers to adopt even smaller clipping ratios to further reduce PAPRs but without compromising the BER performances; 3) the DFT-hybrid case can save at least one quantization bit in comparison with the hybrid case; 4) the hybrid DFT-spread OFDM-DFMA PONs are promising for implementation in cost-sensitive 5G networks; and 5) The proposed PON can reduce the transceiver DSP complexity because of the reduction in minimum required DAC/ADC bit resolution. This enables the decrease in data processing-induced latency at physical layer (the effect of the additional K-point DFT and IDFTs on latency is negligible). As a direct result, the proposed PON is expected to reduce the overall latency between the OLT and ONUs in comparison with the hybrid OFDM-DFMA PONs under the same network operation conditions.

IV. CONCLUSIONS

The novel hybrid DFT-spread OFDM-DFMA PONs have been proposed and numerically investigated for the first time, and performance comparisons have been made for representative 25km SSMF IMDD hybrid OFDM-DFMA PONs with and without incorporating the DFT-spread technique. The proposed network maintains all the salient features associated with the hybrid OFDM-DFMA PONs, in particular, they additionally reduce the upstream signal PAPRs by >2dB. As a direct result, in comparison with the hybrid

improves the fibre transmission performance, but also increases the performance robustness to quantization noise caused by the bit resolution-limited DAC/ADC, as well as relaxing the stringent requirements on linear dynamic operation ranges of transceiver-embedded optical/electrical devices. This statement is confirmed in Fig.3 (a), where BERs versus DAC/ADC quantization bit are illustrated utilizing the parameters in Table I. It is clear that the DFT-hybrid case can reach BERs below the FEC limit of 1E-3 when the resolution bits are as small as 6, while for the hybrid case, the minimum DAC/ADC resolution bits required for achieving the similar performance are

OFDM-DFMA PONs, the proposed PONs increase the upstream system power budget by >3dB and reduce the minimum required DAC/ADC quantization bits by at least 1 bit. The research work suggests that the hybrid DFT-spread OFDM-DFMA PONs are promising for implementation in cost-sensitive 5G networks.

Experimental verifications of the proof-of-principle of the proposed PON are currently being undertaken, along with detailed explorations of the impacts of ONU-embedded practical device characteristics on the upstream PON performance. These characteristics may include, for example, clock frequency offset and phase noise. The corresponding results will be reported in due course.

REFERENCES

[1] ITU-R Recommendation M.2083-0, IMT Vision – Framework and overall objectives of the future development of IMT for 2020 and beyond, Sep.,2015.
[2] Cisco V.N.I "Cisco visual networking index: forecast and trends, 2017–2022," White Paper, Cisco, Nov. 2018. [Online], Available:https://www.cisco.com/c/en/us/solutions/collateral/serviceprovider/visual-networking-index-vni/white-paper-c11-741490.html.
[3] A. Otaka, J. Terada, J. Kani, and K.-I. Suzuki, "Solutions for Future Mobile Fronthaul and Access-Network Convergence," J. Light. Technol. Vol. 35, Issue 3, pp. 527-534, vol. 35, no. 3, pp. 527–534, Feb. 2017.
[4] X. Liu and F. Effenberger, "Emerging Optical Access Network Technologies for 5G Wireless [Invited]," *J. Opt. Commun. Netw*,, vol. 8, no. 12, pp. B70-B79, 2016.
[5] G. Talli et al., "SDN Enabled Dynamically Reconfigurable High Capacity Optical Access Architecture for Converged Services," in *J. Lightwave Technol.*, vol. 35, no. 3, pp. 550-560, 1 Feb. 2017.
[6] N. Cvijetic, "Optical network evolution for 5G mobile applications and SDN-based control," 16th Int. Telecommun. Netw. Strateg. Plan. Symp. Networks 2014, pp. 1–5, 2014.
[7] H. F. Arrano and C. A. Azurdia-Meza, "OFDM: today and in the future of next generation wireless communications," *IEEE Central America and Panama Student Conference* (CONESCAPAN), pp. 1–6. 2016.
[8] Y. Dong, R. Giddings, and J. Tang, "Hybrid OFDM-Digital Filter Multiple Access PONs*," J. Lightwave Technol*., vol. 36, no. 23, pp. 5640-5649, Dec.1, 2018.
[9] M. Bolea, R. P. Giddings, M. Bouich, C. Aupetit-Berthelemot, and J. M. Tang, "Digital filter multiple access PONs with DSP-enabled software reconfigurability", IEEE J. Opt. Commun. Netw, vol. 7, no. 4, pp. 215-222, Apr. 2015.
[10] Y. Rahmatallah and S. Mohan, "Peak-To-Average Power Ratio Reduction in OFDM Systems: A Survey and Taxonomy," *IEEE Communications Surveys & Tutorials*, vol. 15, no. 4, pp. 1567-1592, Fourth Quarter 2013.
[11] T. Jiang and Y. Wu, "An Overview: Peak-to-Average Power Ratio Reduction Techniques for OFDM Signals," *IEEE Transactions on Broadcasting,* vol. 54, no. 2, pp. 257-268, June 2008.
[12] H. G. Myung, J. Lim and D. J. Goodman, "Single carrier FDMA for uplink wireless transmission," *IEEE Vehicular Technology Magazine*, vol. 1, no. 3, pp. 30-38, Sept. 2006.
[13] S. A. Aburakhia, E. F. Badran, D. A. Mohamed, "Distribution of the PAPR for real-valued OFDM signals", *Proc. Int. Conf. Inf. Technol*., pp. 1-8, May 2009.
[14] B. E. Priyanto, H. Codina, S. Rene, T. B. Sorensen, and P. Mogensen, "Initial performance evaluation of DFT-spread OFDM based SC-FDMA for UTRA LTE uplink," *Proc. IEEE Veh. Tech. Conf*., Dublin, Ireland, pp. 3175–3179, Apr. 2007.
[15] R. Giddings, "Real-time digital signal processing for optical OFDM-based future optical access networks," *J. Lightwave Technol*., vol. 32, Issue 4, pp. 553-570, vol. 32, no. 4, pp. 553–570, Feb. 2014.
[16] X.Q. Jin and J.M. Tang, "Experimental investigations of wavelength spacing and colorlessness of RSOA-based ONUs in real-time optical OFDM PONs," *J. Lightwave Technol.,* vol.30, no.16, pp.2603-2609, August 2012.